Development of peptide impregnated V/Fe bimetal Prussian blue analogue as Robust nanozyme for colorimetric fish freshness assessment

Amir Hossein Sharifnezhad , Kheibar Dashtian , Fereshteh Amourizi , Rouholah Zare-Dorabei [*]

Research Laboratory of Spectrometry & Micro and Nano Extraction, Department of Chemistry, Iran University of Science and Technology, Tehran, 16846-13114, Iran

HIGHLIGHTS

- A peptide impregnated V/Fe Bimetal Prussian Blue Analogue was prepared to develop a non-enzymatic strategy.
- A PBA(V/Fe)/INS NSs act as a high peroxidase mimic bio-heterojunction for food spoilage monitoring.
- The PBA(V/Fe)/INS NSs bio-heterojunction can be extended to real sample detection.
- As-proposed sensing strategy responding quickly to the interfacial antioxidant hindrance.

GRAPHICAL ABSTRACT
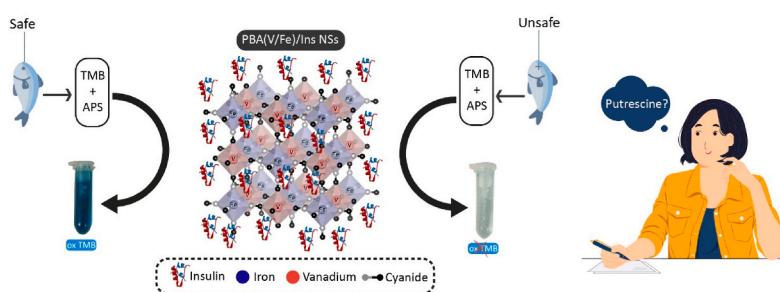
ARTICLE INFO

ABSTRACT

Colorimetric sensing is a low-cost and visual method for food freshness monitoring. We prepared a Vanadium–Iron Prussian blue analogue ($V_{1/5}Fe(CN)_6$ PBA) impregnated with insulin (INS), as a peroxidase-like mimetic probe toward 3,3′5,5′-tetramethylbenzidine (TMB) oxidation and colorimetric monitoring of fish freshness. A specific chemical reaction between putrescine as spoilage marker and the Vanadium–Iron $V_{1/5}Fe(CN)_6$PBA impregnated with insulin ($V_{1/5}Fe(CN)_6$PBA/INS) induces a decreasing peroxidase-like activity of the $V_{1/5}Fe(CN)_6$PBA/INS, generating lower amounts of oxidized products of TMB. The proposed bio-strategy achieved highly sensitive responses in the range of 30 nM to 12 μM toward putrescine with a detection limit of 9.0 nM and outstanding stability, reproducibility, and selectivity. The freshness of five different types of fish samples determined and produces a noticeable color change consistent with the stale fish around the 10 μM, which can warn the oldness of the fish. This new strategy of integration between peptide and multi-metal PBA with intensified enzyme-like mimetics activity may be highly meaningful for thoroughly monitoring the amount of fish freshness.

1. Introduction

Food safety and food quality are in the range of crucial challenges that humans' are kind-faced with it while monitoring harmful compounds is a highly mentioned solution for these challenges [1–4]. Forasmuch as food preservation is complicated especially seafood's due to a gap between fishing to packaging or even, in some cases, selling package less and need to long-term storage of these food products can affect the spoilage process and make it fast, so need to a safe visual sensor which can directly determine food spoilage in very first steps to help a safe and rapid decision
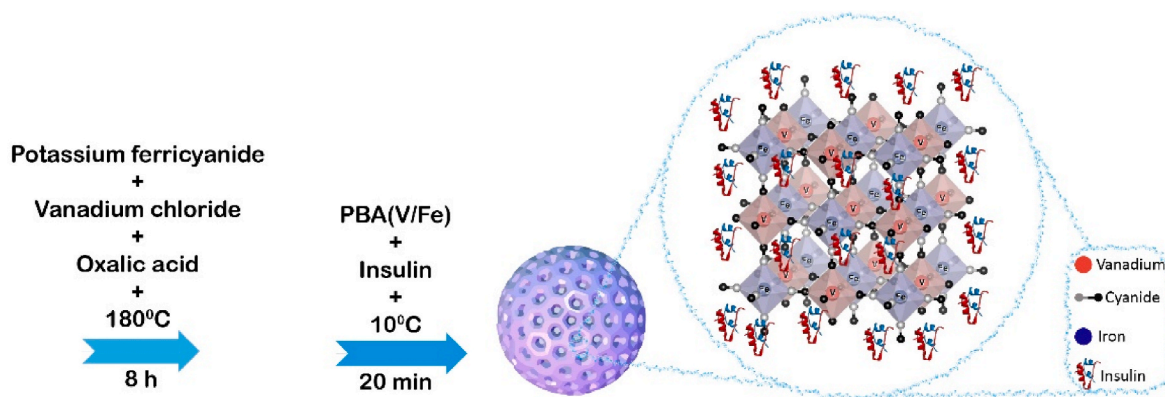
Fig. 1. Schematic illustration for $V_{1/5}Fe(CN)_6PBA/INS$ preparation.

for food industries is necessary [5–9], although their freshness after packaging is also very necessary [10–12]. Freshness assessment of seafood products and shelf-life prediction with sensory methods, along with chemical indicators of fish spoilage is one of the most cost-effective methods ever, compared with financial and health losses, which will happen in the future [13]. Enzymatic autolysis [14], lipid oxidation [15] and hydrolysis [16], non-enzymatic oxidation [17], microbial activity, volatile organic compounds [18] and biogenic amines (BAs) [19] are determined as some important indicators in this category. BAs for their production in a standard environment, e.g. even in absence of bacteria or very low temperature, compared with other spoilage factors puts them in a prime place for sea product analysis [20–22]. Putrescine (Put) is a BA which produces in most kinds of fish, no matter fish is pelagic or non-pelagic and this property put that in the priority of detection for food industries [23]. The early decomposition of fish started at about 0.9 mg/kg and 20 mg/kg of fish have unacceptable quality and spoiled [24]. The development of a convenient and sensitive Put detection strategy is therefore a primary task not only in food quality practices but also for biological mechanism understanding. Conventional approaches to monitoring Put are fluorescent [25], surface-enhanced Raman spectroscopy (SERS) [26] and colorimetric [27] methods which have been reported to provide direct or indirect responses. Amongst, indirect colorimetric strategies based on unconventional metal-containing with enzymatic properties for oxidation of chromogenic probes such as TMB (3,3′,5,5′-Tetramethylbenzidine), o-phenylenediamine and 2,2′-azino-bis(3-ethylben- zothiazoline-6-sulfonic acid) diammonium salt (ABTS) creating a colorimetric signal is a hot topic and practical strategy [28,29]. Other than conventional materials, such as gold nanoparticles, gold nanoclusters, and graphene quantum dots, the metallopolymers (MPs) that are engrossing materials due to combining the advantages of both, polymers and metal centers have also developed [30–32]. The main part of MPs includes coordination polymers (CPs) and metal-organic framework (MOF) with various dimensions for any intended application [33]. CPs with subdivision of porous coordination polymers (PCPs) have undergone extensive study owing to the flourishing demand for nanoporous structures with organic/inorganic linkers and bridges and metal cation nodes to create excellent morphologies [34]. Prussian blue analogues (PBAs) with the replacement of one or two iron ions by another metal ion create metal hexacyanometallates that possess unique crystallographic and chemical specifications [35]. For improving the fantastic attributes of PBAs and profit from synergistic effects, heterostructures of PBA with complex architecture are proposed by researchers [30,31,36,37]. For instance, the vanadium ions with different oxidation states from 2^+ to 5^+ and in some cases as enzyme active centers in living creatures, due to their non-toxicity, make them a convenient option for hybridizing with PBA for the desired goal [38]. Herein, this novel kind of PBAs constituted with vanadium (PBA(V/Fe)) was proposed for some limited applications while other kinds of heterostructure PBAs have been widely investigated

[39–42]. In general, artificial enzymes such as nanozymes as a cost-effective alternative with effective and stable function and simple synthesizing methods have been specially researched and improved year by year and demonstrate great potential for sensing applications. One of the most advantageous peroxidase-like nanozymes is PBs and PBAs as an environmentally friendly alternative. Nanosize structure of PBAs, due to remarkable metal to metal charge transfer between two transition metal ions bio-applications such as biosensors, bioreactors, and even detoxification of humankind fully developed. Some reports introduce PBAs' as a successful peroxidase mimetic or PBAzyme used in sensors [43]. Functionalization of synthesized PBAzyme for detecting specifically depends on the kind of analyte that could be chosen. The peptide as a candidate for end-capping PBAzyme's between other kinds of capping agents such as biomolecules, polymers and enzymes is a promising approach [44]. The kind of peptide for achieving specific targeting is important, for example, insulin peptides are one of the most attractive types due to their bioactivity, biodegradability and good biocompatibility over biogenic amines [45]. In particular, for biogenic amine as an organic base substance that affects human health and food safety, chemical and electrochemical methodologies for sensing are proposed. While rapid detection of these amines such as putrescine as a poisonous substances for human health is necessary. Herein, we report a colorimetric sensor based on $V_{1/5}Fe(CN)_6PBA$ functionalized with insulin hormone as a peroxidase agent for determining putrescine in fish samples. The developed colorimetric sensor was fully characterized by microscopic and spectroscopic methods and was applied for putrescine detection evaluation of the fish product.

2. Experimental section

2.1. Materials

The applied Vanadium(III) chloride (VCl_3, 99.40%), Potassium ferricyanide ($C_6N_6FeK_3$, 99.40%), Oxalic acid anhydrous (C2H2O4, 97.35%), 3,3′,5,5′-Tetramethylbenzidine ($C_{16}H_{20}N_2$), Ammonium persulfate (($NH_4)_2S_2O_8$), methionine ($C_5H_{11}NO_2S$), aspartic acid ($C_4H_7NO_4$), Phenylacetate ($C_8H_8O_2$), Insulin hormone, hydrochloride acid (HCl), sodium hydroxide (NaOH), phosphate saline buffer (PBS) pellet, methionine (Met), aspartic acid (AsA), L-tyrosine (L-Ty), L-arginine (L-Arg), glutathione (Glu), ethylenediamine (EDA), 1,6 diamino hexane (DAH), Histamine (HA), Indole, creatinine, maleic acid (MA), dibutylamine (DBA), diethanolamine (DEA), di-sec-butylamine (DsBA), ethanolamine (EA), tetradecylamine (TDA), triethylenetetramine (TETA) and trimethylamine (TMA) were purchased from Sigma-Aldrich and Merck companies. All received chemicals were used without further purification.
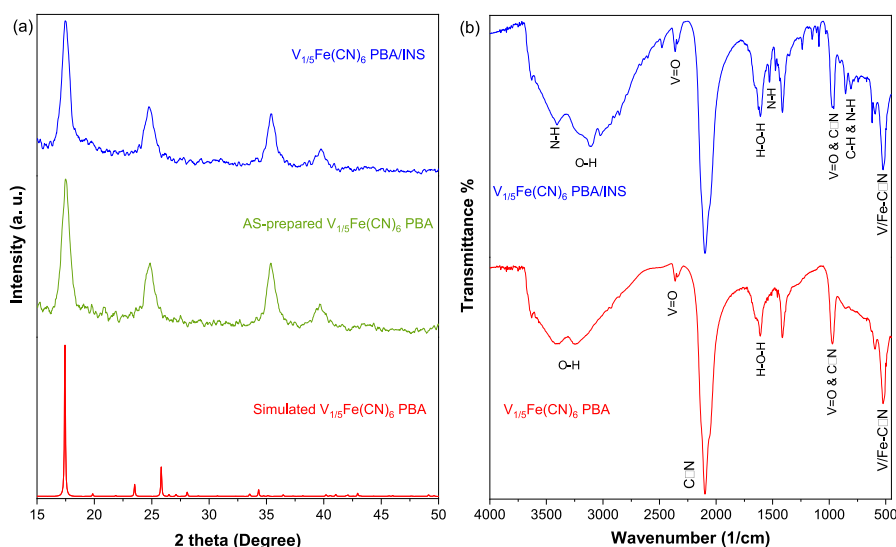
Fig. 2. XRD pattern (a) and FT-IR spectra (b) of $V_{1/5}Fe(CN)_6$PBA and the $V_{1/5}Fe(CN)_6$PBA/INS samples.

2.2. Apparatuses

The colorimetric absorbance peaks were measured by a UV–Visible spectrophotometer with a typical quartz cell (TG-80+ PG instrument, England). FE-SEM images for morphology observation taken by FE-SEM: Sigma, Zeiss, Jena, Germany. The EDX spectrum of various samples, obtain with energy-dispersive X-ray spectrometry (EDX) detector (Oxford INCA II). The structure of crystals was investigated by XRD, PW 1880, Philips, Amsterdam, Netherland. FT-IR spectra were recorded by Perkin Elmer 1720-x setup. Graphical representation of structures was exploited by employing VESTA software.

2.3. Syntheses of $V_{1/5}Fe(CN)_6$PBA

$V_{1/5}Fe(CN)_6$PBA were prepared by the hydrothermal method according to the procedure reported in the previous report [38] as follows: 0.45 g Vanadium (III) chloride, 0.65 gr potassium hexacyanoferrate (III), and 0.81 g anhydrous oxalic acid was added to 40 mL deionized water, respectively. The mixture was ultrasonicated sequentially for 1 h till the solution color changed to red. Then, the mentioned solution was transferred to an autoclave reactor and hydrothermal processing was performed for 8 h at 180 °C. After reaching the autoclave to ambient temperature, the resulting precipitate was gathered with centrifuging (8000 rpm, 10 min) and washed three times with ethanol and water 3:1. Finally, the obtained $V_{1/5}Fe(CN)_6$PBA were dried overnight at 90 °C.

2.4. Impregnation of insulin on $V_{1/5}Fe(CN)_6$PBA

0.7 g of as-synthesized $V_{1/5}Fe(CN)_6$PBA and 20 μL insulin (0.07 mg) were poured into 40 mL water (about 10 M) and mixed for 20 min in an ultrasonic bath with 10 °C temperature. After that, the mixture was incubated at room temperature for 12 h and the final precipitate was washed with ethanol and dried for further use. The final, $V_{1/5}Fe(CN)_6$PBA/INS solution was kept in the refrigerator for further use. All steps for PBA(V/Fe)/INS preparation were illustrated in Fig. 1.

2.5. Preparation of fish samples

Among various fish samples, the freshly smoked fish, trout fish, and tuna fish samples for determination of putrescine were purchased from local markets in Narmak, Tehran, Iran. The samples are suitable for preparation onboard as below. 1.0 g of each type of fish product was homogenized for 15 min in 5.0 mL of 0.4 M $HClO_4$ solution and subsequently sonicated for 30 min. Finally, mixtures were centrifuged at 8000 rpm for 10 min and the supernatant was collected for analysis (the rest of the supernatant was kept at −20 °C for standby).

2.6. Colorimetric measurements

The colorimetric measurements were performed as follows: the specified volume of 0.2% W/V $V_{1/5}Fe(CN)_6$PBA/INS NPs as nanozyme (900–1000 μL), 1 mM TMB as a sensitive peroxidase chromogen substrate (100–800 μL) and 1.75 mM APS as a strong oxidizing agent (100–400 μL) in the presence of Britton–Robinson buffer solution (1 M, pH 7.0) in the presence and absence of different putrescin concentration was mixed to reach the determined volume of 3 mL. After an optimized time, the $V_{1/5}Fe(CN)_6$PBA/INS NPs were removed and UV–Vis spectra of the final solution were recorded.

3. Results and discussion

3.1. Structure and morphology characterization

The X-ray diffraction patterns (XRD) of powder samples were investigated for phase composition identification (Fig. 2a). In the XRD pattern of PBA(V/Fe) NPs, the appeared peaks at 2θs of 17.46°, 24.85°, 29.24°, 35.38°, 39.64°, 43.31°, 50.30°, 54.10° and 56.91°, are related to the crystal plane of (200), (220), (222), (400), (420), (422), (440), (600) and (620) crystal plane, respectively which properly matched with JCPDS 42–1440 card number and simulated pattern of $V_{1/5}Fe(CN)_6$ phase [38]. After insulin loading on $V_{1/5}Fe(CN)_6$ PBA, XRD pattern change does not show any change in the crystal network and that's how insulin simply impregnated on porous structure of $V_{1/5}Fe(CN)_6$.

For investigation of functional groups of $V_{1/5}Fe(CN)_6$ before and after impregnation of insulin, Fourier transforms infrared spectroscopy (FT-IR) has been performed (Fig. 2b). In $V_{1/5}Fe(CN)_6$ FT-IR spectrum, the distinctive bond of $V_{1/5}Fe(CN)_6$ positioned between 500 and 600 cm^{-1} shows stretching bonds of metal with cyanide groups, likewise, appearing bond at 990 and 2100 cm^{-1} is related to the stretching vibration of V=O and C≡N, respectively [46–48]. The observed bond at 1610 and 3500 cm^{-1} corresponded to the and vibration and stretching O–H of the incorporated water molecule in the $V_{1/5}Fe(CN)_6$ structure. After loading insulin on $V_{1/5}Fe(CN)_6$ the associated bond on 1189, 1236 and 1620 cm^{-1} shows the attendance of C≡N stretching, C–O stretching, and tertiary amide in the insulin structure as a characteristic peak of amino acid-based materials. Other observed bonds are related to in-ring
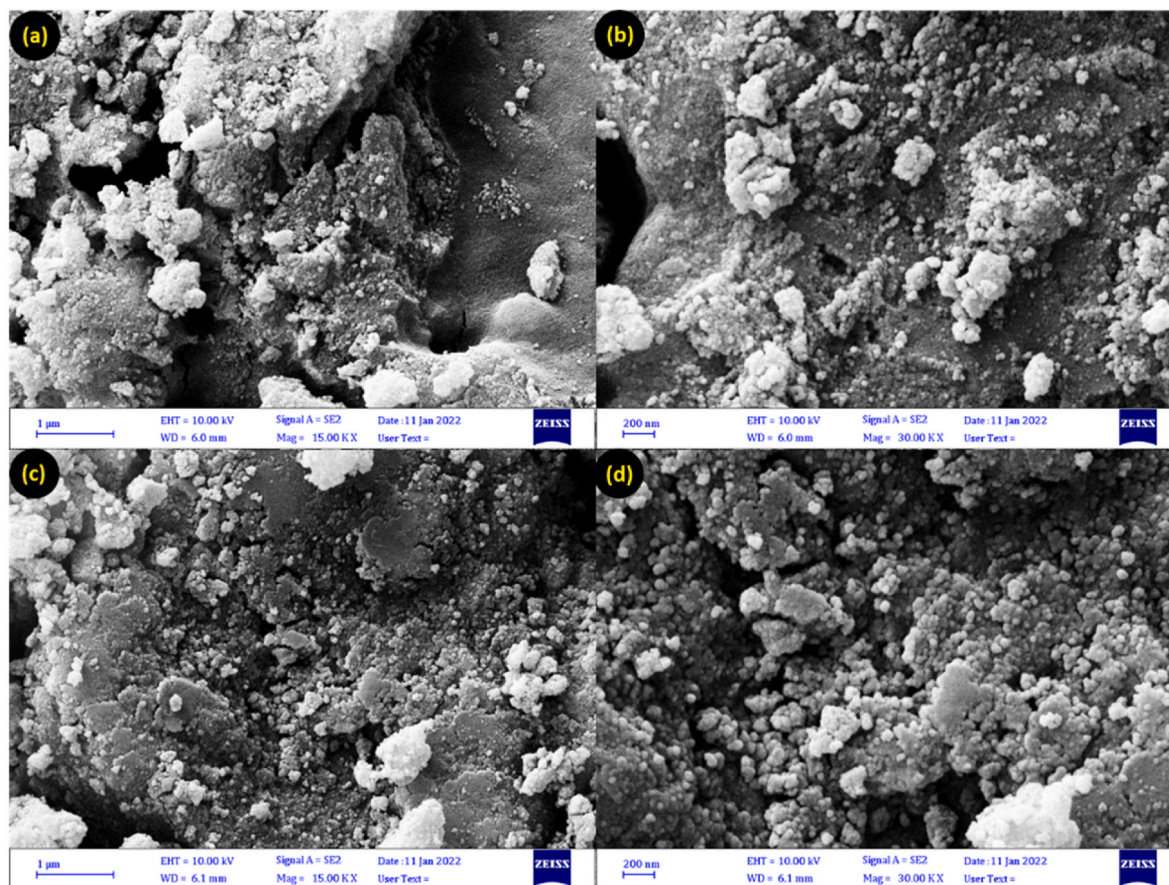
Fig. 3. FE-SEM images of $V_{1/5}Fe(CN)_6PBA$ (a and b) and $V_{1/5}Fe(CN)_6PBA/INS$ (c and d) at different magnification.
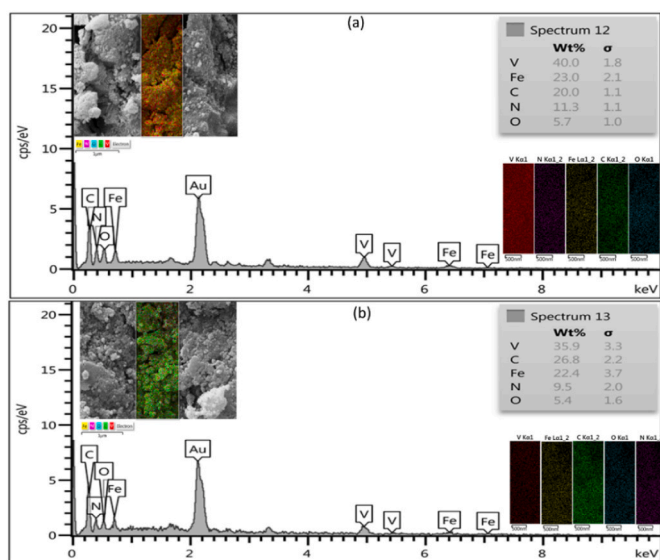

Fig. 4. EDS spectra of $V_{1/5}Fe(CN)_6PBA$ (a) and $V_{1/5}Fe(CN)_6PBA/INS$ (b) (related mapping is inset).

and out-of-ring N–H groups, C–H groups, C═O, C–O, C–C, C═C and N═O groups of insulin. In addition to the success of the synthesis of $V_{1/5}Fe(CN)_6PBA/INS$, the stability of $V_{1/5}Fe(CN)_6$ was confirmed.

The surface morphology of $V_{1/5}Fe(CN)_6PBA$ and $V_{1/5}Fe(CN)_6PBA/INS$ samples was investigated by FESEM at different magnifications (Fig. 3). The obtained PBA(V/Fe) have smooth and regular nanoparticles

due to the intrinsic gravitational force of Fe–O in the structure small accumulation has occurred (Fig. 2a and b). After insulin impregnation, the better particle distribution is due to the reduction of the inherent gravitational force and particles are completely flat manner (Fig. 3c and d). Therefore, the presence of insulin helps to decrease aggregation and gain better results. EDS spectrum in Fig. 4 presents V, Fe, C, N and O existence in both samples and confirms the elemental composition while increases in C percentage after normalizing of the data confirm the loading of Insulin.

3.2. Optimization of sensor elements

To achieve the best response through the as-prepared biosensing strategy, one needs to study every single material's visible spectrum effect and choose an optimized value. In this regard, the effect of insulin on the $V_{1/5}Fe(CN)_6PBA/INS$ nonenzymatic properties and TMB oxidation was investigated and the corresponding UV–Vis spectrum revealed a higher intensity of $V_{1/5}Fe(CN)_6PBA$ and $V_{1/5}Fe(CN)_6PBA/INS$ than that of $V_{1/5}Fe(CN)_6PBA$ which is due to the synergistic effect of insulin peptide and increase of reactive sites for TMB interaction and subsequently intensify oxidation reaction (Fig. 5a).

The $V_{1/5}Fe(CN)_6PBA/INS$ dosage in the range of 0.5–1.3% W/W is demonstrated in TMB oxidation and signal production (Fig. 5b). As revealed with an increase in $V_{1/5}Fe(CN)_6PBA/INS$ dosage TMB oxidation and subsequent intensified absorbance peak which is due to enhancement of catalytic and enzymatic active sites because of the presence of Fe/V multi-oxidation number metals. Therefore, a 1% W/W dosage was selected as the optimal value due to reaching 95% of the UV–Vis signal.

The effect of TMB concentration as a chromogenic agent between 0.05 mM and 0.35 mM was studied and 0.2 mM was selected as a
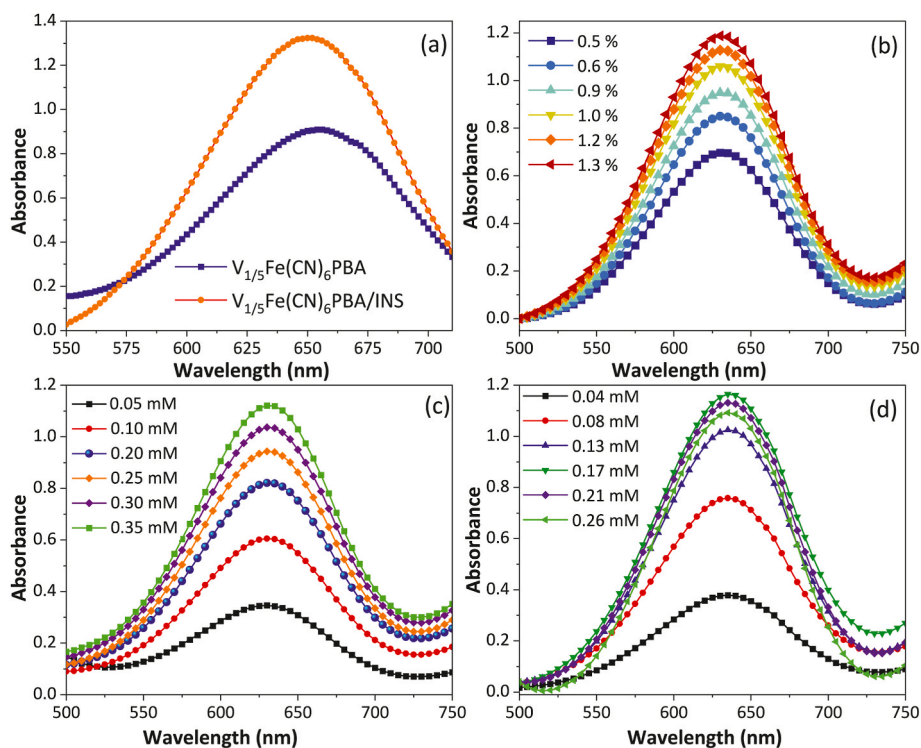
Fig. 5. Effect of insulin adding (a), $V_{1/5}Fe(CN)_6PBA/INS$ dosage (b), TMB concentration (c) and APS concentration (d) on TMB oxidation and readout signal.
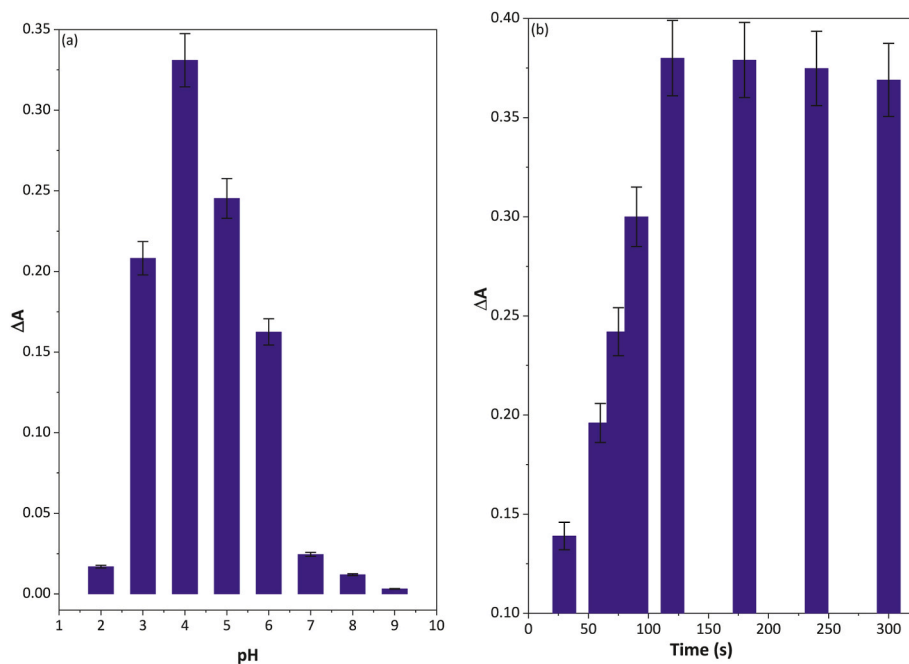

Fig. 6. Different pH at the differential of related absorbance (a), different time at the differential of related absorbance (b) in the presence of 4.5 μM Put (replicates number = 3).

reasonable concentration (Fig. 5c). The lower concentration of TMB was not successful to give an appropriate and precious response, due to there being no required amount of TMB to have a complete color change (Fig. 5c). Also, in high TMB values, the ratio of TMB to catalytic active site has remained constant.

The effect of the APS oxidizer concentration agent revealed that 0.17 mM of APS has an optimum effect on the sensor while in a more concentrated amount APS has a negative effect and causes destruction of

$V_{1/5}Fe(CN)_6PBA/INS$ surface (See Fig. 5d).

3.3. Optimization of the operational factor on sensor responses

Another necessary optimization factor on sensor responses and specifically on nanozyme activity of $V_{1/5}Fe(CN)_6PBA/INS$ are pH and response time. As seen in Fig. 6a, the optimal pH value was found to be 4.0, which is the best pH value for TMB oxidation as well as $V_{1/5}Fe$
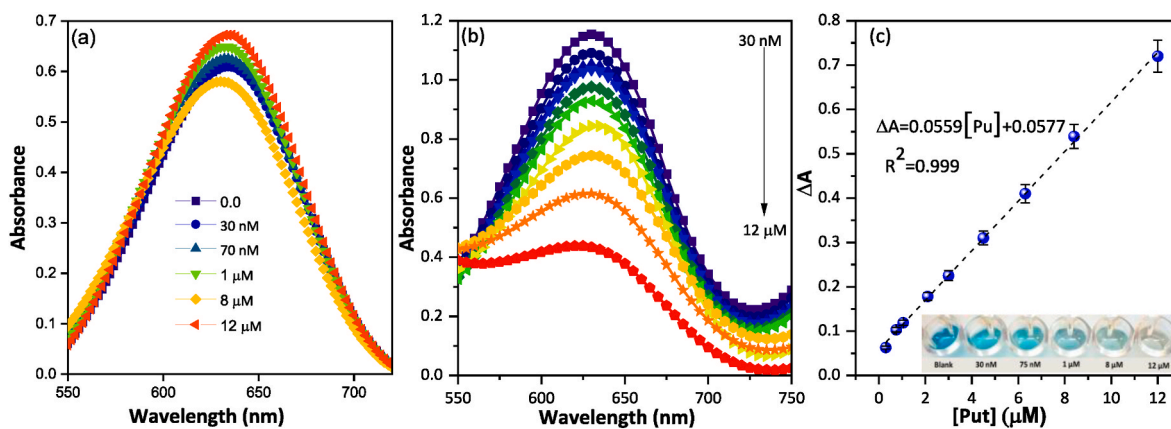
Fig. 7. UV–Vis absorbance spectra ox-TMB on $V_{1/5}Fe(CN)_6PBA$ and $V_{1/5}Fe(CN)_6PBA/INS$ (b) at different Put concentrations and related linear calibration curve for $V_{1/5}Fe(CN)_6PBA/INS$ (n = 3) (c) (the photograph of the sensor in the presence of a different concentration of Put is inset).
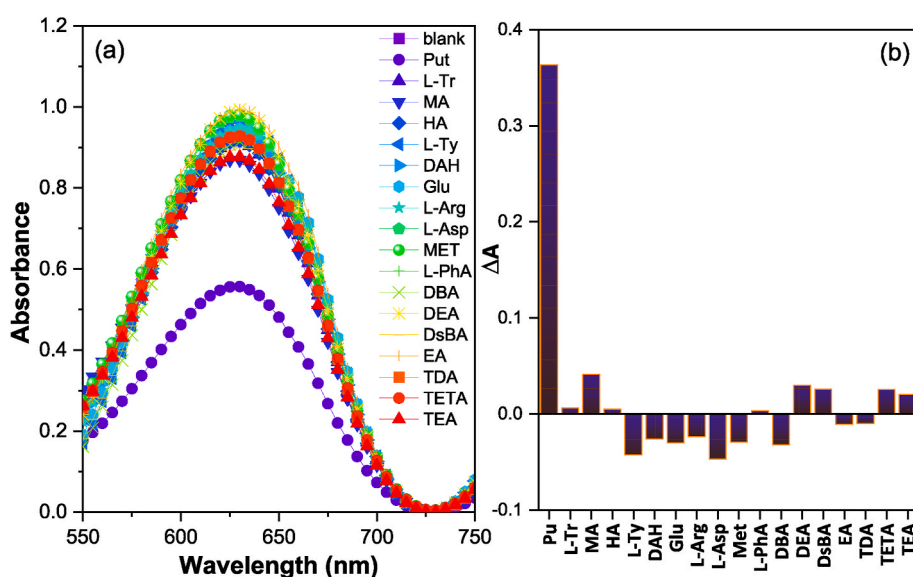
Fig. 8. UV–Vis's absorbance spectra ox-TMB on $V_{1/5}Fe(CN)_6PBA/INS$ in presence of different interference agents (a) and related differential from the blank spectrum (n = 3) (b).
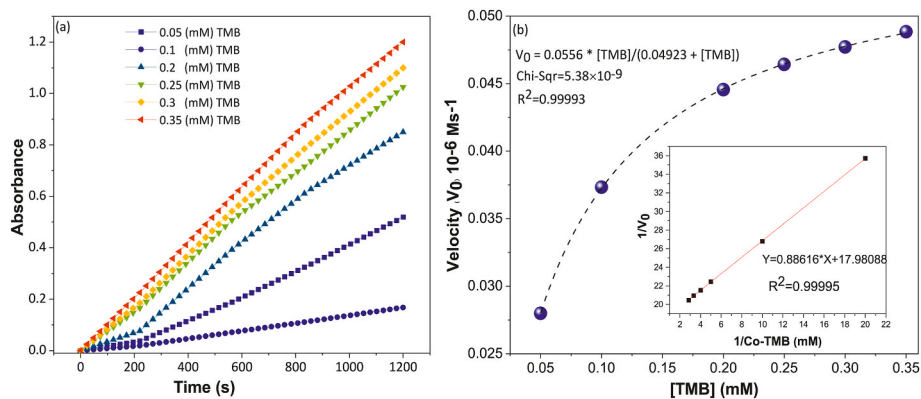
Fig. 9. Time-dependent absorbance changes of TMB at 630 nm of different TMB concentrations (a) and Steady-state kinetic analyses using the Michaelis–Menten model (b) and Lineweaver–Burk model (insets).

$(CN)_6PBA/INS$ and Put interaction. Increasing the response time over 120 s had no meaningful change, thus it is the best time for reaction (Fig. 6b).

3.4. Figures of merits

The sensitivity of sensing applications is vital and this concept can be

Fig. 10. Schematic depiction of enzymatic $V_{1/5}Fe(CN)_6PBA/INS$ sensing process toward Put.

Table 1
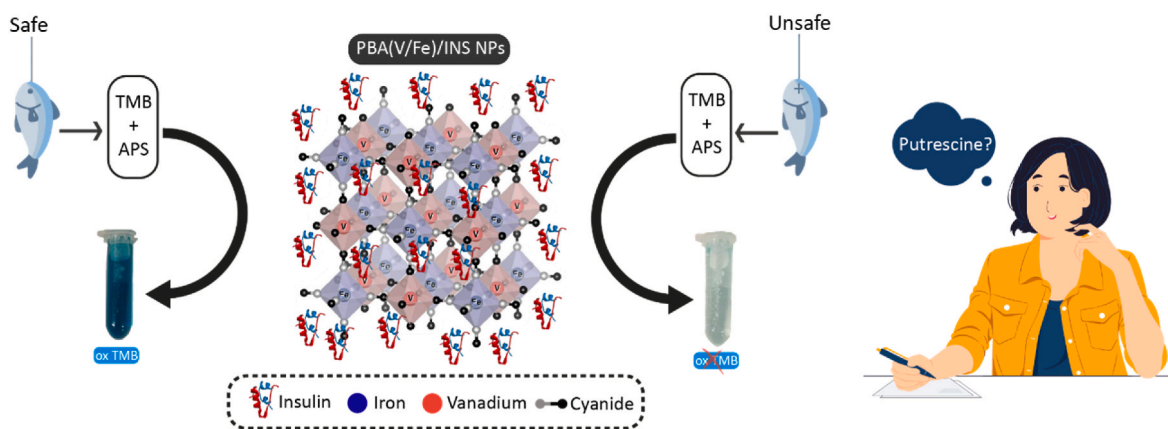The comparison of the proposed sensor with some reported sensors for Put detection.

Samples	Added value (μM)	Founded value (μM)	Recovery %	RSD % (n = 3)
Smoked fish	0.0	13.43 (12.95 HPLC)	-	3.78
	0.5	13.92	98.00	4.65
	2.0	15.45	101.00	4.12
	3.5	17.05	103.42	3.46
	5.0	18.67	104.80	3.34
Trout fish	0.0	15.00 (16.47 HP:C)	-	4.23
	0.5	15.50	100.00	4.45
	2.0	17.06	103.00	3.87
	3.5	18.35	95.71	3.56
	5.0	19.81	96.20	4.23
Tuna fish	0.0	13.00 (15.32 HPLC)	-	3.07
	0.5	13.48	96.00	3.37
	2.0	15.10	105.00	4.25
	3.5	16.58	102.28	3.32
	5.0	18.01	100.20	3.68
Mullet fish	0.0	14.00 (13.01 HPLC)	-	3.5
	0.5	14.50	100.00	4.56
	2.0	16.09	104.50	4.23
	3.5	17.56	101.74	3.8
	5.0	19.17	103.40	3.46
White fish	0.0	13.55 (15.69 HPLC)	-	4.2
	0.5	14.13	96.00	4.32
	2.0	15.63	99.00	3.58
	3.5	17.17	100.57	3.37
	5.0	18.63	99.60	4.9

realized by dispersing $V_{1/5}Fe(CN)_6PBA$ NPs and $V_{1/5}Fe(CN)_6PBA/INS$, APS and TMB in buffer solution and introducing different concentrations of the Put under the optimal reaction conditions (Fig. 7a and b). Putrescin as a polyamine acts as an antioxidant and a reductant to promote oxTMB reduction [49,50]. As revealed, when Put was added,

the solution changed from yellow to colorless and only had a low absorption peak at 630 nm as well as color changes of corresponding samples can be clearly distinguished by the naked eyes. According to Fig. 7c, there was a linear relationship between the decrease of absorbance and concentration of Put ranging from 30 nM to 12 μM ($\Delta A = 0.0559[Put]+0.0557$, $R^2 = 0.999$). The detection limit of Put is up to 9.0 nM (3σ/slope), and the repeatability of the sensor in the absence and presence of analyte was studied which was (RSD$\leq$ 2.69%) and (RSD$\leq$ 3.17%), respectively. Therefore, a sensing platform based on $V_{1/5}Fe(CN)_6PBA/INS$ can provide a simple and convenient method for the visual detection of Put.

From another point of view, the selectivity of the sensor in common biological interfering species was exanimated for their effects on Putrescin detection, methionine (Met), aspartic acid (AsA), L-tyrosine (L-Ty), L-arginine (L-Arg), glutathione (Glu), ethylenediamine (EDA), 1,6 diamino hexane (DAH), Histamine (HA), Indole, creatinine, maleic acid (MA), dibutylamine (DBA), diethanolamine (DEA), di-sec-butylamine (DsBA), ethanolamine (EA), tetradecylamine (TDA), triethylenetetramine (TETA), trimethylamine (TMA). The result in Fig. 8a and **b** indicate that interference studies confirmed the susceptibility of this system to the as-mentioned compounds.

3.5. The kinetic study

To the consideration of enzyme activity and to find the interdependence between $V_{1/5}Fe(CN)_6PBA/INS$ and enzyme kinetic parameters, the Michaelis–Menten ($V_0 = (V_{max}[S])/(Km + [S])$) behaviors were studied with TMB as substrates. Where V_0 is the initial velocity, V_{max} is the maximal reaction velocity, $[S]$ is the concentration of TMB substrate and K_m is the Michaelis constant [51,52]. A series of nanonzymatic experiments on $V_{1/5}Fe(CN)_6PBA/INS$ was carried out by changing the concentration of TMB substrate and keeping the other parameter constant at a different time (Fig. 9a). The reaction rates of TMB oxidation were calculated and the typical Michaelis–Menten curves were plotted (Fig. 9b). By nonlinear fitting of Michaelis–Menten plot, the kinetic parameters V_{max} and K_m were obtained which was validated by Lineweaver–Burk plots of $1/v$ vs $1/[S]$ (**See** Fig. 9b). Generally, K_m is an

Table 2
Comparison of analytical parameters of the proposed sensor with other reported sensors of putrescine.

Material used	Sensing mechanism	Linear range	Limit of detection	Analysis time	Ref
Putrescine oxidase	Electrochemical	0.01–0.25 mM	5 μM	2 min	[57]
Bisphthalocyanine and polypyrrole	Electrochemical	1–100 μM	0.34 M	-	[58]
o-phthalaldehyde and thioglycolic acid	Colorimetric	0.8–200 μM	0.44 μM	12 min	[59]
p-type PFTPDOBT polymer with triphenodioxazine	Electrochemical	0–80 mg L^{-1}	9.0 mg L^{-1}	5 s	[60]
1,4-butanediol	Colorimetric	0.01–10 mg L^{-1}	2.0 μg L^{-1}	40 min	[61]
$V_{1/5}Fe(CN)_6PBA/INS$	Colorimetric	30 nM-12 μM	9.0 nM	120 s	This work

indicator of affinity between the enzyme and substrate where lower K_m value revealed superior affinity and catalytic activity as well as applied for comparison of the enzyme-like performance of different nanozymes. Our results revealed that $V_{1/5}Fe(CN)_6PBA/INS$ had a low binding affinity towards TMB, and high binding affinity towards ROSs as well as confirmed the oxidase-like activity of $V_{1/5}Fe(CN)_6PBA/INS$.

3.6. The design strategy of $V_{1/5}Fe(CN)_6PBA/INS$ sensor

In Fig. 10, the detection mechanism for colorimetric sensing of $V_{1/5}Fe(CN)_6PBA/INS$ is vividly described. $V_{1/5}Fe(CN)_6PBA/INS$ probe was employed for the unique feature of peroxidase mimic activity towards the chromogenic substrate, TMB [53]. The oxidation process of TMB which causes a colorimetric change in further steps reveals the absence, presence and amount of Putrescine analyte in the measured sample. $V_{1/5}Fe(CN)_6PBA/INS$ catalyze the oxidation reaction by mediating the electron transfer of TMB in the presence of APS to achieve a color change in $\lambda_{max} = 630$ nm which is responsible for the blue color observed during the oxidation of TMB. Introducing putrescine analyte to sensor plays competitive inhibitor role for TMB molecules towards $V_{1/5}Fe(CN)_6PBA/INS$ nanozyme which cause diminish the blue observed color while in the high concentration of putrescin, sensor colorimetric change fades. Based on this inhibition concept, we have developed a colorimetric strategy for the quantification of putrescine. To clarify the details of engineered nanozyme, the reason for choosing each material should be expressed. Vanadium–Iron as multi-oxidation number containing compounds is recognized as insulin enhancer agents which opt as PBA co-precursor to achieve accurate results while analyte is easily exported from samples [54–56]. Besides that, the impregnation of insulin on $V_{1/5}Fe(CN)_6PBA/INS$ for increasing putrescine export is a bio-inspired method that is regulated by mammalian cells.

3.7. Analytical performances

A designed sensor was employed for the detection of putrescine in smoked fish, trout fish, whitefish, mullet fish, and tuna fish samples, and proofed the application of the sensor in real samples. In this regard, a standard addition method with a specific concentration of putrescine for spiking was selected (Table 1). The result exhibits the required recovery percent (95.71–104.80%) for putrescine determination in real fish samples while the amounts Put in the pure samples are in good agreement with those of the measurement by HPLC. Compared with the other colorimetric sensors (Table 2), our strategy has high simplicity and visual resolution and revealed satisfactory and comparable results in terms of LOD, linear range and analysis time as well as in material preparation and mechanism.

4. Conclusions

In conclusion, insulin impregnated on the vanadium/iron bimetal-based Prussian blue analogues ($V_{1/5}Fe(CN)_6PBA/INS$) was successfully prepared and applied as an effective and accurate nanozyme for mimicking peroxidase activity for fast quantification of putrescine as the biogenic amine in seeing food with the naked eye or common colorimetric method. Minimum reagents, high peptide loading capacity, ease for probe fabrication with good reproducibility, selectivity, sensitivity, fast response, and wide linear range with improved lower detection limit are some of the countable features of our proposed PBA-based sensor. This strategy can be directly applied and a selective alternative for putrescine and food spoilage monitoring, as well as bimetal PBAs supports can be utilized for sensing different interests and applicable analytes after suitable modification.

CRediT authorship contribution statement

Amir Hossein Sharifnezhad: Writing – original draft, and, Data

curation, Formal analysis, Writing – review & editing. **Kheibar Dashtian:** Data curation, Formal analysis, Writing – review & editing. **Fereshteh Amourizi:** Writing – original draft, and, Data curation, Formal analysis, Writing – review & editing. **Rouholah Zare-Dorabei:** Supervision, Funding acquisition, Writing – review & editing.

Declaration of competing interest

The authors declare that they have no known competing financial interests or personal relationships that could have appeared to influence the work reported in this paper.

Data availability

No data was used for the research described in the article.

References

[1] Y. Huang, X. Mu, J. Wang, Y. Wang, J. Xie, R. Ying, E. Su, The recent development of nanozymes for food quality and safety detection, J. Mater. Chem. B 10 (9) (2022) 1359–1368.
[2] H. Yousefi, H.-M. Su, S.M. Imani, K. Alkhaldi, C.D.M. Filipe, T.F. Didar, Intelligent food packaging: a review of smart sensing technologies for monitoring food quality, ACS Sens. 4 (4) (2019) 808–821.
[3] C. Griesche, A.J. Baeumner, Biosensors to support sustainable agriculture and food safety, TrAC, Trends Anal. Chem. 128 (2020), 115906.
[4] F. Mustafa, S. Andreescu, Chemical and biological sensors for food-quality monitoring and smart packaging, Foods 7 (10) (2018) 168.
[5] M.E. Genovese, S. Abraham, G. Caputo, G. Nanni, S.K. Kumaran, C. D. Montemagno, A. Athanassiou, D. Fragouli, Photochromic paper indicators for acidic food spoilage detection, ACS Omega 3 (10) (2018) 13484–13493.
[6] Z. Ma, P. Chen, W. Cheng, K. Yan, L. Pan, Y. Shi, G. Yu, Highly sensitive, printable nanostructured conductive polymer wireless sensor for food spoilage detection, Nano Lett. 18 (7) (2018) 4570–4575.
[7] L.R. Magnaghi, G. Alberti, C. Milanese, P. Quadrelli, R. Biesuz, Naked-eye food freshness detection: innovative polymeric optode for high-protein food spoilage monitoring, ACS Food Sci. Technol. 1 (2) (2020) 165–175.
[8] P.K. Prabhakar, S. Vatsa, P.P. Srivastav, S.S. Pathak, A comprehensive review on freshness of fish and assessment: analytical methods and recent innovations, Food Res. Int. 133 (2020), 109157.
[9] J. Zhang, H. Huang, G. Song, K. Huang, Y. Luo, Q. Liu, X. He, N. Cheng, Intelligent biosensing strategies for rapid detection in food safety: a review, Biosens. Bioelectron. (2022), 114003.
[10] A. Ballester-Caudet, L. Hakobyan, Y. Moliner-Martinez, C. Molins-Legua, P. Campíns-Falcó, Ionic-liquid doped polymeric composite as passive colorimetric sensor for meat freshness as a use case, Talanta 223 (2021), 121778.
[11] N. Jornet-Martínez, Y. Moliner-Martínez, R. Herráez-Hernández, C. Molins-Legua, J. Verdú-Andrés, P. Campíns-Falcó, Designing solid optical sensors for in situ passive discrimination of volatile amines based on a new one-step hydrophilic PDMS preparation, Sensor. Actuator. B Chem. 223 (2016) 333–342.
[12] N. Jornet-Martinez, L. Hakobyan, A.I. Argente-García, C. Molins-Legua, P. Campins-Falco, Nylon-supported plasmonic assay based on the aggregation of silver nanoparticles: in situ determination of hydrogen sulfide-like compounds in breath samples as a proof of concept, ACS Sens. 4 (8) (2019) 2164–2172.
[13] H. Singh, G. Singh, N. Kaur, N. Singh, Pattern-based colorimetric sensor array to monitor food spoilage using automated high-throughput analysis, Biosens. Bioelectron. 196 (2022), 113687.
[14] A.M.B. Rørå, S. Birkeland, L. Hultmann, T. Rustad, T. Skåra, B. Bjerkeng, Quality characteristics of farmed Atlantic salmon (Salmo salar) fed diets high in soybean or fish oil as affected by cold-smoking temperature, LWT–Food Sci. Technol. 38 (3) (2005) 201–211.
[15] J.T. Salonen, K. Seppänen, K. Nyyssönen, H. Korpela, J. Kauhanen, M. Kantola, J. Tuomilehto, H. Esterbauer, F. Tatzber, R. Salonen, Intake of mercury from fish, lipid peroxidation, and the risk of myocardial infarction and coronary, cardiovascular, and any death in eastern Finnish men, Circulation 91 (3) (1995) 645–655.
[16] G.M. Turchini, B.E. Torstensen, W.K. Ng, Fish oil replacement in finfish nutrition, Rev. Aquacult. 1 (1) (2009) 10–57.
[17] A.E. Ghaly, D. Dave, S. Budge, M. Brooks, Fish spoilage mechanisms and preservation techniques, Am. J. Appl. Sci. 7 (7) (2010) 859.
[18] H. Jo, M.-H. Son, S.-H. Seo, Y.-S. Chang, Matrix-specific distribution and diastereomeric profiles of hexabromocyclododecane (HBCD) in a multimedia environment: air, soil, sludge, sediment, and fish, Environ. Pollut. 226 (2017) 515–522.

[19] P.K. Prabhakar, P.P. Srivastav, S.S. Pathak, Kinetics of total volatile basic nitrogen and trimethylamine formation in stored rohu (Labeo rohita) fish, J. Aquat. Food Prod. Technol. 28 (5) (2019) 452–464.

[20] G. Meng, C. Zhang, P. Du, S. Sun, X. Zhang, B. Wang, X. Lu, A dual-channel luminescent signal readout nanoprobe for rapid monitoring of biogenic amines in milk and yogurt, Sensor. Actuator. B Chem. (2022) 131435.

[21] A. Orouji, F. Ghasemi, A. Bigdeli, M.R. Hormozi-Nezhad, Providing multicolor plasmonic patterns with Au@ Ag core–shell nanostructures for visual discrimination of biogenic amines, ACS Appl. Mater. Interfaces 13 (17) (2021) 20865–20874.

[22] L. Tang, S. Liao, J. Qu, Self-healing and multistimuli-responsive hydrogels formed via a cooperation strategy and their application in detecting biogenic amines, ACS Appl. Mater. Interfaces 10 (32) (2018) 27365–27373.

[23] K.H. Kim, C.S. Park, S.J. Park, J. Kim, S.E. Seo, J.E. An, S. Ha, J. Bae, S. Phyo, J. Lee, In-situ food spoilage monitoring using a wireless chemical receptor-conjugated graphene electronic nose, Biosens. Bioelectron. 200 (2022), 113908.

[24] I.A. Bulushi, S. Poole, H.C. Deeth, G.A. Dykes, Biogenic amines in fish: roles in intoxication, spoilage, and nitrosamine formation—a review, Crit. Rev. Food Sci. Nutr. 49 (4) (2009) 369–377.

[25] T. Leelasree, H. Aggarwal, MOF sensors for food safety: ultralow detection of putrescine and cadaverine in protein rich foods, J. Mater. Chem. C 10 (2022) 2121–2127.

[26] J. Sun, Z. Zhang, H. Li, H. Yin, P. Hao, X. Dai, K. Jiang, C. Liu, T. Zhang, J. Yin, Ultrasensitive SERS analysis of liquid and gaseous putrescine and cadaverine by a 3D-rosettelike nanostructure-decorated flexible porous substrate, Anal. Chem. 94 (13) (2022) 5273–5283.

[27] S. Sudalaimani, A. Esokkiya, S. Hansda, C. Suresh, P. Tamilarasan, K. Giribabu, Colorimetric sensing of putrescine and cadaverine using ninhydrin as a food spoilage detection reagent, Food Anal. Methods 13 (3) (2020) 629–636.

[28] L. Zhang, G.P. Yang, S.J. Xiao, Q.G. Tan, Q.Q. Zheng, R.P. Liang, J.D. Qiu, Facile construction of covalent organic framework nanozyme for colorimetric detection of Uranium, Small 17 (44) (2021), 2102944.

[29] G. Fu, S.T. Sanjay, W. Zhou, R.A. Brekken, R.A. Kirken, X. Li, Exploration of nanoparticle-mediated photothermal effect of TMB-H2O2 colorimetric system and its application in a visual quantitative photothermal immunoassay, Anal. Chem. 90 (9) (2018) 5930–5937.

[30] D. Duan, X. Fang, K. Li, A peroxidase-like nanoenzyme based on strontium (II)-ion-exchanged Prussian blue analogue derivative SrCoO3/Co3O4 nanospheres and carbon quantum dots for the colorimetric detection of tigecycline in river water, Talanta 240 (2022), 123112.

[31] G. Zhang, K. Yu, B. Zhou, J. Wang, C. Zheng, L. Qu, H. Chai, X. Zhang, Magnetic zirconium-based Prussian blue analog nanozyme: enhanced peroxidase-mimicking activity and colorimetric sensing of phosphate ion, Microchim. Acta 189 (6) (2022) 1–10.

[32] M.B. Zakaria, T. Chikyow, Recent advances in Prussian blue and Prussian blue analogues: synthesis and thermal treatments, Coord. Chem. Rev. 352 (2017) 328–345.

[33] G.I. Dzhardimalieva, L.N. Rabinskiy, K.A. Kydralieva, I.E. Uflyand, Recent advances in metallopolymer-based drug delivery systems, RSC Adv. 9 (63) (2019) 37009–37051.

[34] A. Muthurasu, G.P. Ojha, M. Lee, H.Y. Kim, Integration of cobalt metal–organic frameworks into an interpenetrated prussian blue analogue to derive dual metal–organic framework-assisted cobalt iron derivatives for enhancing electrochemical total water splitting, J. Phys. Chem. C 124 (27) (2020) 14465–14476.

[35] P.S. Camacho, R. Wernert, M. Duttine, A. Wattiaux, A. Rudola, P. Balaya, F. Fauth, R. Berthelot, L. Monconduit, D. Carlier, Impact of synthesis conditions in Na-rich prussian blue analogues, ACS Appl. Mater. Interfaces 13 (36) (2021) 42682–42692.

[36] N. Akram, W. Ma, J. Guo, Y. Guo, Z. Yansong, A. Hassan, J. Wang, Synergistic catalysis of Fe3O4/CuO bimetallic catalyst derived from Prussian blue analogues for the efficient decomposition of various organic pollutants, Chem. Phys. 540 (2021), 110974.

[37] K. Feng, J. Zhang, H. Dong, Z. Li, N. Gu, M. Ma, Y. Zhang, Prussian blue nanoparticles having various sizes and crystallinities for multienzyme catalysis and magnetic resonance imaging, ACS Appl. Nano Mater. 4 (5) (2021) 5176–5186.

[38] J.H. Lee, G. Ali, D.H. Kim, K.Y. Chung, Metal-organic framework cathodes based on a vanadium hexacyanoferrate Prussian blue analogue for high-performance aqueous rechargeable batteries, Adv. Energy Mater. 7 (2) (2017), 1601491.

[39] W. He, J.M. Cain, M.W. Meisel, D.R. Talham, Interplay between core and shell in a RbCoFe@ RbNiCo Prussian blue analogue spin transition heterostructure, J. Mater. Chem. C 9 (33) (2021) 10830–10840.

[40] Y. Song, X. Zhao, Z.-H. Liu, Surface selenium doped hollow heterostructure/defects Co-Fe sulfide nanoboxes for enhancing oxygen evolution reaction and supercapacitors, Electrochim. Acta 374 (2021), 137962.

[41] E. Mamontova, M. Rodríguez-Castillo, E. Oliviero, Y. Guari, J. Larionova, M. Monge, J. Long, Designing heterostructured core@ satellite Prussian Blue Analogue@ Au–Ag nanoparticles: effect on the magnetic properties and catalytic activity, Inorg. Chem. Front. 8 (9) (2021) 2248–2260.

[42] J. Xing, J. Fu, S. Guan, Y. Zhang, M. Lei, Z. Peng, Novel KV-Fe Prussian blue analogues nanocubes for high-performance aqueous ammonium ion batteries, Appl. Surf. Sci. 543 (2021), 148843.

[43] E.V. Karpova, E.V. Shcherbacheva, M.A. Komkova, A.A. Eliseev, A.A. Karyakin, Core–Shell nanozymes "artificial peroxidase": stability with superior catalytic properties, J. Phys. Chem. Lett. 12 (23) (2021) 5547–5551.

[44] J.J. Hu, D. Xiao, X.Z. Zhang, Advances in peptide functionalization on mesoporous silica nanoparticles for controlled drug release, Small 12 (25) (2016) 3344–3359.

[45] R. Primavera, E. Bellotti, D. Di Mascolo, M. Di Francesco, J. Wang, B.D. Kevadiya, A. De Pascale, A.S. Thakor, P. Decuzzi, Insulin Granule-loaded microplates for modulating blood glucose levels in type-1 diabetes, ACS Appl. Mater. Interfaces 13 (45) (2021) 53618–53629.

[46] K. Itaya, S. Toshima, Electrochemical preparation of a Prussian blue analog: iron-ruthenium cyanide, J. Am. Chem. Soc. 104 (13) (1982) 3751–3752.

[47] C.G. Tsiafoulis, P.N. Trikalitis, M.I. Prodromidis, Synthesis, characterization and performance of vanadium hexacyanoferrate as electrocatalyst of H2O2, Electrochem. Commun. 7 (12) (2005) 1398–1404.

[48] F.A. Miller, C.H. Wilkins, Infrared spectra and characteristic frequencies of inorganic ions, Anal. Chem. 24 (8) (1952) 1253–1294.

[49] R. Sardar, S. Ahmed, N.A. Yasin, Role of exogenously applied putrescine in amelioration of cadmium stress in Coriandrum sativum by modulating antioxidant system, Int. J. Phytoremediation 24 (9) (2022) 955–962.

[50] J. Collado-González, M.C. Piñero, G. Otálora, J. López-Marín, F.M.d. Amor, The effect of foliar putrescine application, ammonium exposure, and heat stress on antioxidant compounds in cauliflower waste, Antioxidants 10 (5) (2021) 707.

[51] S. Cai, Z. Fu, W. Xiao, Y. Xiong, C. Wang, R. Yang, Zero-dimensional/two-dimensional Au x Pd100−x nanocomposites with enhanced nanozyme catalysis for sensitive glucose detection, ACS Appl. Mater. Interfaces 12 (10) (2020) 11616–11624.

[52] A.P. Nagvenkar, A. Gedanken, Cu0. 89Zn0. 11O, a new peroxidase-mimicking nanozyme with high sensitivity for glucose and antioxidant detection, ACS Appl. Mater. Interfaces 8 (34) (2016) 22301–22308.

[53] R.P. Ojha, S. Pal, R. Prakash, Cu-Fe Prussian blue analog nanocube with intrinsic oxidase mimetic behaviour for the non-invasive colorimetric detection of Isoniazid in human urine, Microchem. J. 171 (2021), 106854.

[54] J. Wang, V.G. Yuen, J.H. McNeill, Effect of vanadium on insulin sensitivity and appetite, Metab., Clin. Exp. 50 (6) (2001) 667–673.

[55] S. Treviño, A. Diaz, Vanadium and insulin: partners in metabolic regulation, J. Inorg. Biochem. 208 (2020), 111094.

[56] L. Hawel III, R.R. Tjandrawinata, C.V. Byus, Selective putrescine export is regulated by insulin and ornithine in Reuber H35 hepatoma cells, Biochim. Biophys. Acta Mol. Cell Res. 1222 (1) (1994) 15–26.

[57] B. Bóka, N. Adányi, J. Szamos, D. Virág, A. Kiss, Putrescine biosensor based on putrescine oxidase from Kocuria rosea, Enzym. Microb. Technol. 51 (5) (2012) 258–262.

[58] I. Apetrei, C. Apetrei, Application of voltammetric e-tongue for the detection of ammonia and putrescine in beef products, Sensor. Actuator. B Chem. 234 (2016) 371–379.

[59] X. Qi, W.-F. Wang, J. Wang, J.-L. Yang, Y.-P. Shi, Highly selective colorimetric detection of putrescine in fish products using o-phthalaldehyde derivatization reaction, Food Chem. 259 (2018) 245–250.

[60] J. Zhu, X. Wang, H. Wang, Real-time putrescine detection by triphenodioxazine-based organic thin-film transistor sensor, J. Electron. Mater. 49 (8) (2020) 4691–4696.

[61] X. Ying, A. Kang, X. Zhu, X. Li, Molecular imprint enhanced specific adsorption visualization on electrospun chromogenic membrane for efficient detection of putrescine, J. Appl. Polym. Sci. 136 (45) (2019), 48186.